

## Feature Review

# Synthesis of Large-Area Single-Crystal Graphene

Meihui Wang,<sup>1,2</sup> Da Luo,<sup>1</sup> Bin Wang,<sup>3</sup> and Rodney S. Ruoff<sup>1,2,4,5,\*</sup>

There have been breakthroughs in the mass production of graphene by chemical vapor deposition (CVD) and its practical applications have also been identified. Grain boundaries are typically present in ‘CVD graphene’ and adversely impact its properties. We summarize recent progress in growing large-area single-crystal graphene. Centimeter-scale single-crystal, truly single-layer graphene (SLG) films have been reportedly achieved on single-crystal Cu(111) foils by CVD growth, while meter-scale single-crystal SLG films have been reportedly produced with assistance of a roll-to-roll technique. The growth of uniform single crystals of bilayer or multilayer graphene over a large area remains an exciting challenge. Layer-by-layer transfer and the stacking of single-crystal SLG is considered a promising route to making new types of ‘single’ crystals or quasicrystals with specific numbers of layers and different stacking angles.

## Structure and Properties of Single-Crystal Graphene

Graphene, a single layer of carbon atoms arranged in a honeycomb lattice (Figure 1A), has attracted worldwide attention due to its unique 2D structure and excellent physical properties [1–5]. When two graphene layers are stacked on top of each other, the properties of the bilayer material [6] depend on the stacking angle (Figure 1B,C) [7,8]. **AB-stacked bilayer graphene (BLG)** (see Glossary) reportedly has a continuously tunable **bandgap** of up to 250 meV when a vertical electrical field is applied, which enables the fabrication of semiconductor devices [9–11]. An AB-stacked BLG film was reportedly converted to an ultra-thin ‘diamond’ film (F-diamane) by fluorine chemisorption [12]. In addition, **twisted bilayer graphene (tBLG)** reportedly presents  $\theta$ -dependent interfacial conductivity [13], van Hove singularities [14], and particular electronic structures [15] that are reported to have potential for use in ultra-sensitive sensors and ultra-thin capacitors. A Mott insulator and unconventional superconductivity with a critical temperature up to 1.7 K was reported for a twist angle of  $1.1^\circ$  in BLG [10,11]. Compared with AB-stacked BLG, tBLG reportedly has a higher chemical reactivity, which was said to be due to distinct variations in the density-of-states distribution in the gap region [16].

Among various synthesis methods, **chemical vapor deposition (CVD)** has shown to be the most promising for the scalable production of large-area high-quality graphene films [17]. Ruoff and colleagues first reported the preparation of a centimeter-scale single-layer graphene (SLG) film on a commercial Cu foil by CVD in 2009 [18]. Unlike Ni with high carbon solubility ( $\sim 0.9$  at.% at  $900^\circ\text{C}$  [19]), Cu has a much lower carbon solubility, even up to  $1000^\circ\text{C}$  (7.4 at. ppm at  $1020^\circ\text{C}$  [20]), which is believed to predominantly contribute to the surface-mediated mechanism of graphene growth and good uniformity of the number of layers of the as-grown graphene [21]. As a result, Cu-based foils or films are the most common substrates for studying the behavior of graphene growth by the CVD method and SLG films have been mass produced on copper-based substrates in industry. However, **grain boundaries (GBs)** are often present in the CVD-grown graphene films and are reported to contain 5-, 7-, and/or distorted 6-membered rings (Figure 1D–F) [18,22,23]. They are formed where two (or more) **graphene islands**

## Highlights

Methods for growth of millimeter to centimeter-sized single-crystal, single-layer graphene (SLG) islands have been reviewed. Several strategies have been used to decrease the nucleation density of graphene so as to grow a large-area single-crystal island of SLG from a single nucleus; these are described.

Methods for growth of centimeter to meter-scale single-crystal SLG films have been reviewed. The epitaxial growth of centimeter-scale single-crystal SLG, reliably achieved recently on Cu (111) foils and also with no adlayers, is explained.

By ‘feeding’ carbon atoms by either diffusion at the interface between a graphene layer and the substrate, or diffusion through the substrate from its backside, sub-millimeter single-crystal BLG islands have been made on copper substrates. The growth of hexagonal single-crystal graphene islands with two to eight layers and sizes of hundreds of micrometers on Cu/Ni foils is reviewed.

Large-area single-crystal AB-stacked bilayer/trilayer graphene films have been produced on single-crystal Cu/Ni(111) alloy foils by parametric study as a function of the concentration of Ni in the foils; this method is outlined.

Single-crystal AB-stacked and ‘twisted’ BLG with a predetermined rotation angle has been prepared on a large scale by either stacking or folding large-area adlayer-free single-crystal SLG films; this is presented as a different pathway (if further developed and refined) to multilayer and single-crystal films, including with arbitrary twist angle, in contrast to the ‘as-grown’ multilayer films that are almost always AB-stacked (twist angle of zero).



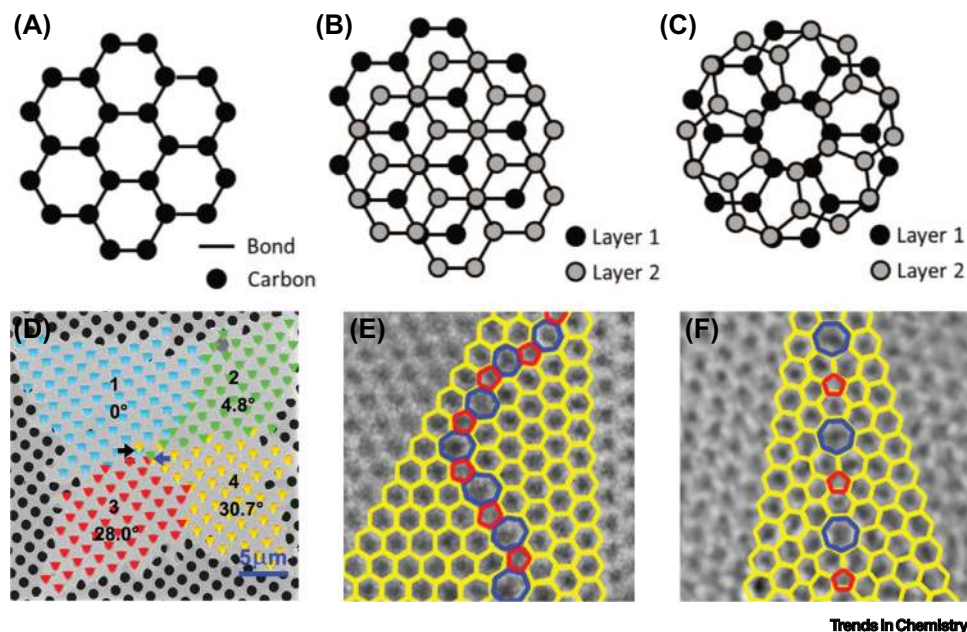


**Figure 1. Structures of Graphene and Grain Boundaries (GBs).** (A) Single-layer graphene, (B) AB-stacked bilayer graphene, and (C) twisted bilayer graphene. (D) Scanning electron microscope image of a large four-lobed graphene island. (E,F) Two types of line dislocations in graphene islands, with pentagonal (red) and heptagonal (blue) rings in the outlined GBs. Images reproduced, with permission, from [6,23].

<sup>1</sup>Center for Multidimensional Carbon Materials (CMCM), Institute for Basic Science (IBS), Ulsan 44919, Republic of Korea

<sup>2</sup>Department of Chemistry, Ulsan National Institute of Science and Technology (UNIST), Ulsan 44919, Republic of Korea

<sup>3</sup>CAS Key Laboratory of Nanosystem and Hierarchical Fabrication, CAS Center for Excellence in Nanoscience, National Center for Nanoscience and Technology, Beijing 100190, PR China

<sup>4</sup>Department of Materials Science and Engineering, Ulsan National Institute of Science and Technology (UNIST), Ulsan 44919, Republic of Korea

<sup>5</sup>School of Energy and Chemical Engineering, Ulsan National Institute of Science and Technology (UNIST), Ulsan, 44919, Republic of Korea

\*Correspondence: [rsruoff@ibs.re.kr](mailto:rsruoff@ibs.re.kr) (R.S. Ruoff).

(grown from different **nuclei**) that have different **orientations** join together [23]. GBs have been reported to lower the thermal, electrical, and mechanical properties of graphene [24–28] and the existence of GBs reportedly influence the stacking order in bi- and multilayers [29]. Consequently, the synthesis of large-area single-crystal graphene (thus, with no GBs) by reliable/reproducible and scalable methods is of great interest.

In this review, we focus on developments in the CVD growth of large-area single-crystal graphene with different numbers of layers on Cu-based substrates, including Cu and Cu-based alloys. Large single-crystal SLG islands have been obtained by several methods on polycrystalline substrates. Recently, centimeter-scale **adlayer**-free single-crystal SLG films have been reproducibly produced on home-made single-crystal Cu(111) foils by removing all the carbon contaminants in the substrates. Mass production of single-crystal SLG films has been achieved by either a roll-to-roll technique or a home-designed pilot-scale CVD system. However, it is still challenging to grow large single-crystal bilayer or multilayer graphene by the CVD method, and layer-by-layer assembly of large-area single-crystal SLG films appears to be a promising way to produce them, especially with defined interlayer rotation angles.

## Growth of Single-Crystal SLG

Based on the number of nuclei formed at the early stage of graphene growth, there are two strategies for the growth of large-area single-crystal SLG. The first is to ensure that graphene growth is from a single nucleus on a polycrystalline substrate, and the second is epitaxial growth from multiple nuclei on a single-crystal substrate (see Table 1).

### Single-Crystal SLG Grown from One Single Nucleus

At an early stage, researchers tried to grow a large-area single-crystal graphene island from a single nucleus on a polycrystalline substrate, based on the fact that, in some situations, the single

graphene island grows epitaxially once it has been nucleated and does not change its lattice orientation when it crosses the GBs of the polycrystalline metal substrate (Figure 2A) [30–32]. Thus, it is critical to control and suppress the nucleation density of graphene, which is reported to be determined by the number of **active sites** and the concentration of active carbon species [formed by the decomposition of CH<sub>4</sub>, e.g., CH<sub>x</sub> (x = 3, 2, 1, 0)] on the substrate surface [33,34].

The surface conditions of the substrate, such as roughness and cleanliness [35–38], and the CVD parameters, including growth temperature [39] and partial pressure of CH<sub>4</sub> (or ratio of H<sub>2</sub>/CH<sub>4</sub>) [40], reportedly influence the nucleation density of graphene. Pretreatment of the metal substrate, including surface polishing, acid etching, and high temperature annealing in a reductive atmosphere, is still widely used to clean and flatten the substrate surface and decrease the number of active sites. A growth temperature (above 1000°C) with a low partial pressure of the carbon precursor that leads to a relatively low concentration of active carbon species was typically used to grow single-crystal graphene islands [37,41,42]. In addition to decreasing the flow rate of the carbon precursor, Li and colleagues showed that by folding a Cu foil to form a ‘pocket’, an extremely low methane partial pressure is achieved inside the pocket and a 0.5-mm single-crystal graphene island with an average growth rate of 6 μm/min could be grown on the interior side of the Cu pocket [40].

In 2013, Hao and colleagues first reported the role of oxygen in the graphene growth process. They showed that oxygen on the Cu surface not only decreases the graphene nucleation density by passivating Cu surface active sites (Figure 2C) but also accelerates the growth of the graphene island by shifting the growth kinetics from edge-attachment-limited to diffusion-limited (Figure 2D) [43]. Individual islands with diameters larger than 1 cm were grown on oxygen-rich Cu foils after a 12-h growth (Figure 2B). Following this, various methods to introduce surface oxygen on Cu foils have been reported, including heating the Cu foil in air [44], annealing it in an inert atmosphere [45], and introducing O<sub>2</sub> during the graphene growth [46], all of which have indicated that the presence of surface oxygen is effective in decreasing the nucleation density of graphene.

Seeding growth is a common method for the synthesis of various single-crystal materials. Graphene oxide flakes [47], exfoliated thin graphite flakes [30], and prepatterned polymethyl methacrylate (PMMA) dots [48] have been used as the seeds for graphene growth on Cu. Wu and colleagues reported the controllable growth of arrays of single-crystal graphene islands with sizes of tens of microns using prepatterned PMMA dots as the nucleation seeds, which might be a promising method for quantity production of single-crystal graphene islands of a certain size (Figure 2E) [48]. A single-crystal graphene film was reported on a polycrystalline Pt foil if graphene islands with aligned orientation were first transferred to the substrate, followed by growth from their edges [49]. The key point of using seeds for graphene growth is to ensure that graphene grows only from the seeds rather than nucleating elsewhere. It should always be remembered that undesired nucleation may occur in the empty space between seeds as a result of the supersaturation of active carbon species formed by decomposition of the carbon source, if the seed density is too low [50].

A 1.5-inch single-crystal graphene island was reportedly obtained on a Cu<sub>85</sub>Ni<sub>15</sub> alloy foil after 2.5-h growth from one single nucleus by locally feeding the carbon precursor through a quartz nozzle (Figure 2F) [51]. A new approach was reported by Vlassiounk and colleagues for the synthesis of a foot-long single-crystal graphene film on a moving polycrystalline Cu<sub>90</sub>Ni<sub>10</sub> alloy foil at rates up to 2.5 cm/h (Figure 2G). With a moving substrate and localized feeding of the carbon precursor, the fastest-growing island orientation reportedly overwhelms any slower-growing islands, resulting in a single-crystal graphene film [52]. It should be noted that localized feeding

## Glossary

### AB-stacked bilayer graphene (BLG):

BLG where half of the atoms in the upper layer lie directly over the center of a hexagon and the other half of the atoms lie directly over an atom in the lower graphene sheet; thus with a ‘0°’ rotation angle between the two layers.

**Active site:** atomic step bunches, grain boundaries, vacancies, adatoms, and impurities on the substrate that the graphene is being grown on.

**Adlayer:** (or adlayer graphene) bilayer or multilayer regions that could be under (typically this has been the case) or perhaps ‘atop’ of the top continuous graphene layer. For example, a single-layer region beneath the continuous layer is called a ‘bilayer region’, accounting for both layers: the finite lower layer (the ‘adlayer’) and the top continuous layer.

**Bandgap:** an energy range in a solid where no electronic state exists, such as between the valance and conduction bands.

**Chemical vapor deposition (CVD):** a method where one or more volatile (i.e., gas phase) precursors are converted to high-quality thin films on the surface of a substrate, typically at high temperature or perhaps in a plasma.

**CVD protocol:** parameters in the CVD process, including type of target substrate; time-temperature program; pressure and gas species and their flow rates.

**Grain boundary (GB):** the region between two grains in a polycrystalline material. For graphene, a ‘2D’ material, grain boundaries are regions containing 5-, 7-, and/or distorted 6-membered rings of carbon atoms and can be approximately thought of as ‘lines’ between the 2D grains (grains are sometimes referred to as ‘domains’ for the 2D materials).

**Graphene fold:** a three-layer thick ribbon-like structure formed by (single-layer) graphene wrinkling and ‘folding over’ onto the substrate, such as we have found can happen during cooling from the growth temperature (~1000°C) to room temperature, due to a ‘build-up’ of compressive interfacial stress from the thermal contraction of the substrate.

**Graphene island:** an isolated graphene region, typically with a size from several micrometers to a few centimeters.

of the carbon precursor can be used only for a Cu/Ni alloy with proper composition and is not suitable for the graphene growth on pure Cu or pure Ni. This might be due to the fact that the nucleation density of graphene on the Cu/Ni alloy is much lower than that on Cu under the same conditions [53] and that the carbon solubility of Cu/Ni alloys (such as Cu<sub>85</sub>Ni<sub>15</sub> or Cu<sub>90</sub>Ni<sub>10</sub>) is not high enough to dissolve all the carbon in the substrate bulk [54].

Since graphene grows from a single nucleus, it is usually time consuming to produce a large single crystal. Recently, several strategies have been reported for accelerating the growth of single-crystal graphene islands, including stacking Cu foils to create molecular flow in a confined

**Nucleus/nuclei:** critical nucleus size for graphene growth is said to be at about 20–24 C atoms and is suggested to be smaller than 1 nm in size.

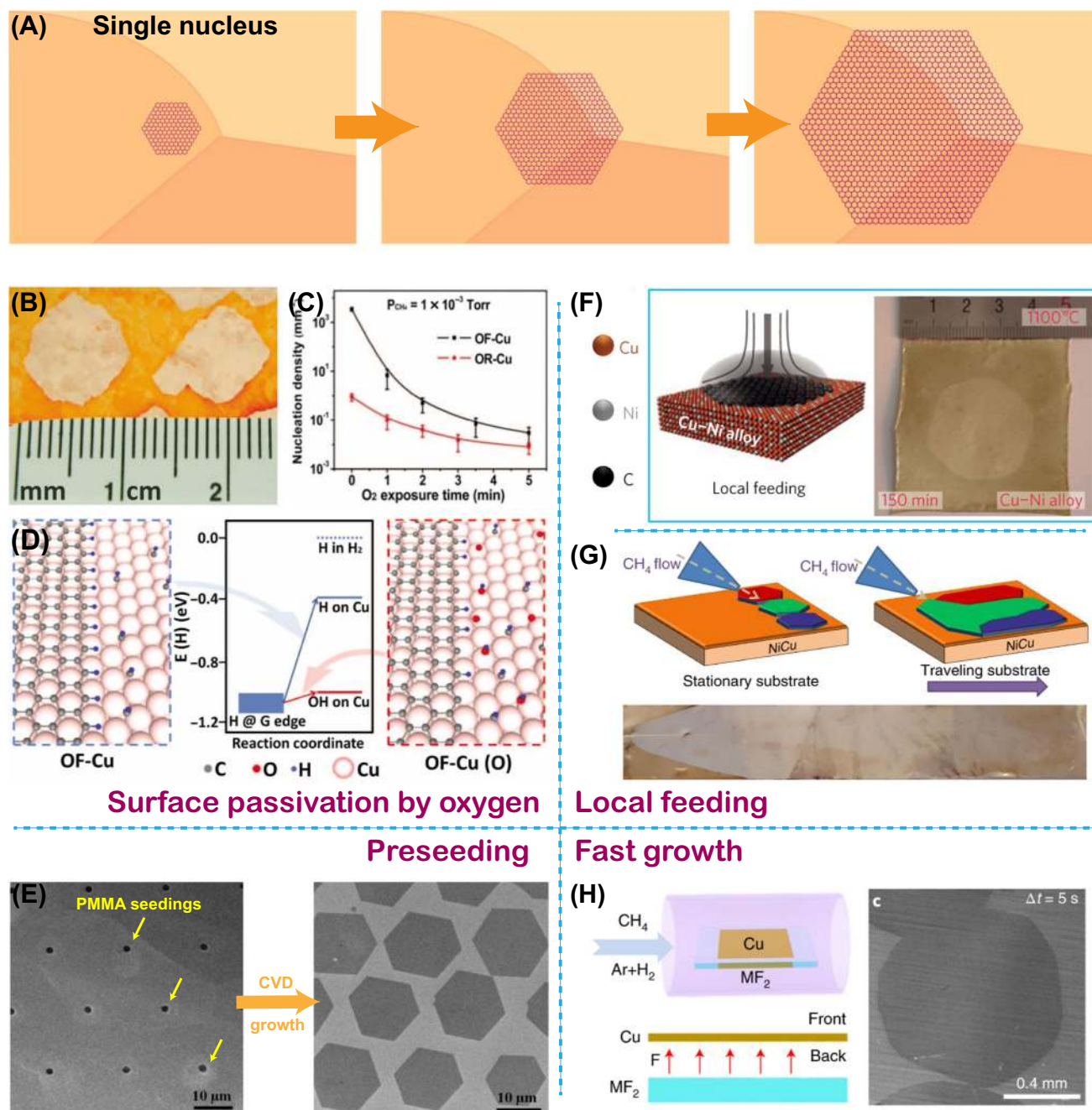
**Orientation:** the direction of graphene zig-zag (or armchair) edges.

**Twisted bilayer graphene (tBLG):** bilayer graphene where one layer is rotated relative to the other with a non-zero rotation angle. (AB-stacked bilayer graphene is, thus, not referred to as 'twisted')

Table 1. Representative Studies on the Growth of Large-Area Single-Crystal SLG

Strategy	Method	Summary of reported method	Reported substrate <sup>a</sup>	Reported size	Reported growth time	Year	Refs
Single nucleus	Surface smoothing	Annealing in Ar/H <sub>2</sub> for 3 h	Poly-Cu	0.4 mm	~15 min	2012	[42]
		Electro-polishing and suppressing Cu evaporation by stacking foils	Poly-Cu	2 mm	6 h	2013	[37]
		Melting Cu followed with resolidification	Poly-Cu	1 mm	5 h	2013	[38]
	Optimizing CVD parameters	Cu enclosure with low carbon supply	Poly-Cu	0.5 mm	~90 min	2011	[40]
		Long-time annealing, a controlled pressure, relatively high growth temperature, and low methane pressure	Poly-Cy	2.3 mm	125 min	2012	[36]
		Annealing in a non-reducing environment, low reactor pressure, and high H <sub>2</sub> /CH <sub>4</sub> ratio	Poly-Cu	5 mm	48 h	2013	[87]
	Oxygen passivation	O <sub>2</sub> treatment at 1035°C for 5 min	O-rich poly-Cu	1 cm	12 h	2013	[43]
		Annealing in Ar before growth	Poly-Cu	5.9 mm	~10 h	2013	[45]
		Heating in air at 200°C for 20 min	Poly-Cu	3 mm	3 h	2015	[44]
		Introducing O <sub>2</sub> during growth	Poly-Cu	1 cm	20 h	2016	[46]
	Seeding	Using PMMA dots as seeds	Poly-Cu	18 μm	20 min	2011	[48]
		Using graphene oxide flakes as seeds	Poly-Cu	150 μm	20 min	2014	[47]
	Local feeding	Local feeding and multistep supply of methane	Poly-Cu <sub>85</sub> Ni <sub>15</sub> alloy	3.8 cm	2.5 h	2016	[51]
	Evolutionary selection	Locally feeding carbon source to a moving substrate	Poly-Cu <sub>90</sub> Ni <sub>10</sub> alloy	~30 cm	~12 h	2018	[52]
	Fast growth	A molecular flow in a confined space with assistance of oxygen	Single-crystal Cu (100) foil	3 mm	10 min	2016	[55]
		Multistage carbon supply and second passivation	Single-crystal Cu (100) foil	4 mm	100 min	2016	[56]
		Continuously supply oxygen from oxide substrate	Poly-Cu	0.3 mm	5 s	2016	[58]
		Continuously supply fluorine from metal fluoride substrate	Poly-Cu	1 mm	5 s	2019	[59]
Multiple nuclei	'Seamless stitching' of aligned graphene islands on single-crystal substrates	Magnetron sputtering on single-crystal MgO(111)	Cu(111) film	—	10 min	2012	[62]
		Repeated chemomechanical polishing and annealing	Cu(111) foil	3 × 6 cm <sup>2</sup>	1 h	2015	[68]
		Temperature-gradient-driven annealing	Cu(111) foil	5 × 50 cm <sup>2</sup>	20 min	2017	[70]
		Magnetron sputtering	Cu(111) film	4 inch	2 h	2017	[69]
		Electroplating Ni onto Cu(111) foils followed with annealing at 1050°C for 4–6 hours	Cu/Ni(111) foils (1.3 to 8.6 at.% Ni)	2 × 8 cm <sup>2</sup>	5 min	2018	[54]
		Contact-free annealing	Cu(111) foil	32 cm <sup>2</sup>	1 h	2019	[72]
		Two-step magnetron sputtering	Cu <sub>90</sub> Ni <sub>10</sub> (111) film	4 inch	10 min	2019	[71]

<sup>a</sup>Abbreviation: Poly, polycrystalline.



Surface passivation by oxygen

Local feeding

Preseeding

Fast growth

Trends in Chemistry

**Figure 2. Strategies for Single-Crystal Single-Layer Graphene (SLG) Island Production by the Single-Nucleus Method.** (A) Schematic of the mechanism of single-crystal SLG growth from a single nucleus. (B) Optical image of centimeter-scale graphene islands on oxygen-rich Cu. (C) Graphene nucleation density as a function of  $\text{O}_2$  exposure time. (D) Energies of different configurations of H attachment, calculated by density functional theory. (E) Scanning electron microscope (SEM) images of patterned polymethyl methacrylate (PMMA) dots and the as-grown array of graphene islands formed by subsequent chemical vapor deposition (CVD). (F) Illustration of the configuration of local feedstock feeding and the synthesized single-crystal graphene island. (G) Illustration of the evolutionary selection mechanism and the as-grown single-crystal graphene film. (H) Schematic of the configuration used for the reported fast growth of single-crystal graphene islands and an SEM image of the as-grown millimeter-scale graphene islands. The copper foil is placed directly on the top of a metal fluoride substrate ( $\text{MF}_2$ ; M = Ba, Ca, or Mg) with a small gap of 10–20  $\mu\text{m}$  between them. Images adapted, with permission, from [43,48,51,52,59]. Abbreviations: OF-Cu, oxygen-free Cu; OR-Cu, oxygen-rich Cu.

space [55], using a two-step carbon-source supply (CSS) that applies a low CSS for the nucleation stage and increases it for the subsequent growth stage for rapid growth [56], using what was stated to be a more active carbon source such as ethane [57] as compared with methane, and continuously introducing oxygen or fluorine to help the decomposition of methane [58,59]. Growth rates of more than hundreds of micrometers per minute have been reported. Liu and colleagues reported a 1-mm graphene island achieved in 5 s by a local supply of fluorine from a metal fluoride substrate, with a growth rate as fast as 200  $\mu\text{m}/\text{min}$ , as shown in Figure 2H [59]. Despite this, the size of graphene grown using the single nucleation method is, at this time, limited to hundreds of microns to a few centimeters and complicated processes or equipment are needed.

#### Single-Crystal SLG Grown from Multiple Nuclei

The other strategy is to epitaxially grow aligned graphene islands on single-crystal substrates. Single-crystal Cu(111) surface is reported to be a good candidate due to its sixfold symmetry and small lattice mismatch with graphene ( $\sim 4\%$ ) [60,61]. Graphene islands aligned in a specific direction have been reported on the Cu(111) surface [62–64], while graphene islands oriented in two or three directions were observed on Cu(100) [62] and Cu(110) surface [65], which have fourfold and twofold symmetries, respectively. Several theories have been reported to explain the alignment of graphene on Cu(111), such as graphene edge–metal interaction [32], step-attach growth [66], and embedded growth mode [67]. The growth of a centimeter-scale (or even meter-scale) single-crystal graphene film is reportedly very fast, less than or equal to 2 h [54,68–72].

The preparation of large-area single-crystal metal substrates is thus crucial for the epitaxial growth of single-crystal graphene. Nguyen and colleagues reported an 18  $\text{cm}^2$  Cu(111) foil using a process that includes repeated chemical-mechanical polishing and annealing [68]. Xu and colleagues reported a temperature-gradient-driven annealing method to convert meter-scale polycrystalline Cu foils into Cu(111) foils with assistance of a roll-to-roll technique (Figure 3A,B) [70]. Their theoretical calculations indicated that the GBs of Cu are premelting at 1300 K and the temperature gradient at the liquid/solid phase interface drives the migration of GBs in a preferred direction. Jin and Ruoff invented a contact-free annealing method to produce large-area single-crystal metal foils from commercial polycrystalline metal foils (Figure 3C) [73]. By minimizing the contact stresses during annealing, single-crystal Cu(111), Ni(111), Co(0001), Pt(111), and Pd(111) foils, with grain sizes up to 32  $\text{cm}^2$ , were produced (Figure 3C–E). Single-crystal Cu/Ni(111) foils with various Ni concentrations have also been produced using this home-made Cu(111) foil by a two-step method; first the desired amount of Ni was electroplated onto the Cu(111) foil and it was then annealed at 1050°C for 4–6 h (Figure 3F) [54].

Besides foils, single-crystal Cu(111) and Cu/Ni(111) films have also been reported in recent years [69,71,74,75]. Ago and colleagues reported a Cu(111) film with twins by magnetron sputtering of copper on c-plane sapphire [76]. Later, the same group reported a heteroepitaxial Cu(111) film without twins by sputtering Cu on a single-crystal MgO(111) substrate heated at 500°C [62]. Deng and colleagues reported a 4-inch single-crystal Cu(111) film by magnetron sputtering of copper on a single-crystal sapphire, which was preannealed in pure oxygen for 12 h (Figure 3G) [69]. It was reported that a  $\text{Cu}_2\text{O}$  buffer layer with a thickness of 1–2 nm was formed at the interface between Cu and oxygen-pretreated sapphire, which reportedly released the stress induced by the lattice mismatch between Cu and sapphire and resulted in a twin-free single-crystal Cu(111) film (Figure 3H). In addition, wafer-scale Cu/Ni(111) films were reported on single-crystal sapphire substrates by either sputtering using CuNi alloy as the target and co-sputtering Cu [74] or Ni film in sequence [71] (Figure 3I).

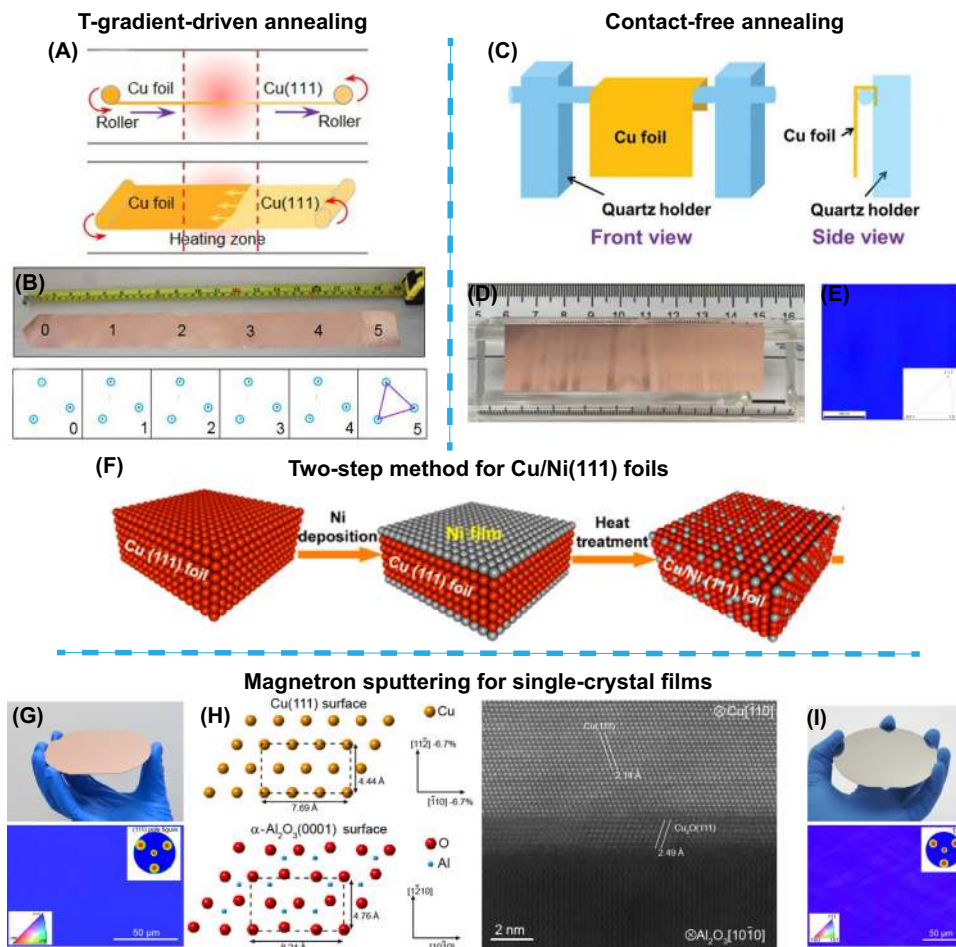
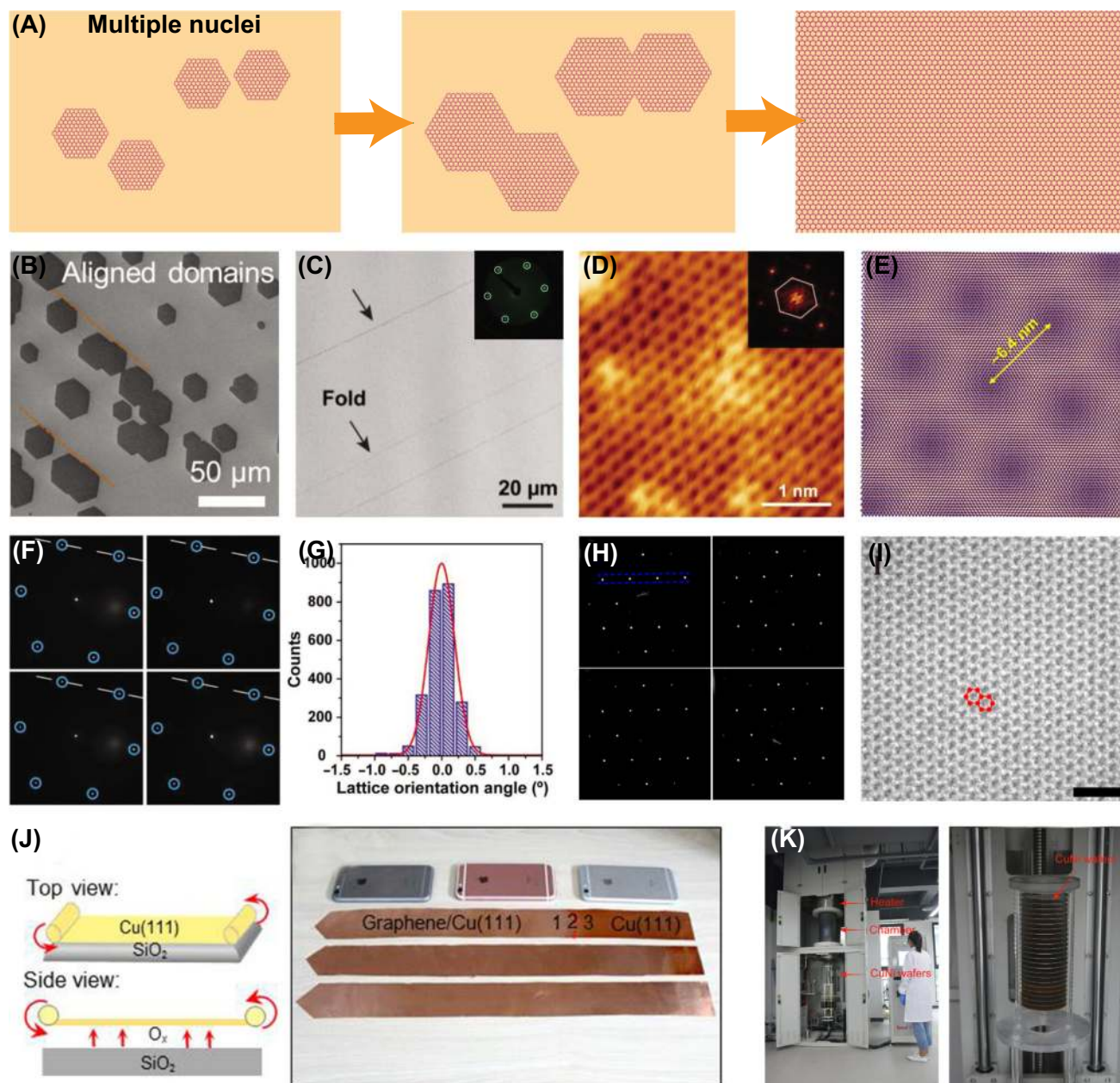


**Figure 3. Methods for Obtaining Single-Crystal Cu(111) and Cu/Ni(111) Alloy Substrates.** (A) Schematic of the reported continuous production of a single-crystal Cu(111) foil by the temperature-gradient-driven method. (B) Photograph of the as-obtained Cu(111) foils over 5 × 50 cm and reported representative low-energy electron diffraction patterns from six different regions. (C) Schematic of the contact-free method for single-crystal metals, with a quartz holder from which the metal foil is suspended. (D) Photograph and (E) electron backscatter diffraction (EBSD) map of the reported as-obtained single-crystal Cu foil. The inset in (E) is the inverse pole figure of the EBSD map. (F) Schematic of the reported preparation of the Cu/Ni(111) foils by a two-step method. (G) Photograph and EBSD map of the reported single-crystal Cu(111) film prepared by magnetron sputtering. (H) Schematic of the orientation relationship between Cu(111) and oxygen-terminated  $\alpha\text{-Al}_2\text{O}_3(0001)$  and transmission electron microscopy image of the interface regions of Cu/ $\alpha\text{-Al}_2\text{O}_3$ . (I) Photograph and EBSD map of the reported single-crystal  $\text{Cu}_{60}\text{Ni}_{10}(111)$  film prepared by magnetron sputtering. Image reproduced, with permission, from [54,69–73].

Based on the achievements of single-crystal substrates, the growth of large-area single-crystal SLG films have been reported by several groups [54,68–72,75]. Ogawa and colleagues reported a highly oriented SLG film on a heteroepitaxial Cu(111) film, the single orientation of which was confirmed by dark-field low-energy electron microscopy (LEED) over 1 mm<sup>2</sup> [62]. Nguyen and colleagues reported ‘seamless stitching’ in atomic scale of two aligned graphene islands grown on a Cu(111) surface, as shown in Figure 4A, using scanning tunneling microscopy (STM), selected area electron diffraction (SAED), and optical microscopy after UV treatment [68]. We note that the graphene film grown on Cu(111) foils made by contact-free annealing is single crystal (Figure 4B,C) over a large area and does not contain any adlayers [72]. It was found that the amount



Trends in Chemistry

**Figure 4. Multiple-Nuclei Strategy for Producing a Large-Area Single-Crystal Single-Layer Graphene (SLG) film.** (A) Schematic of the epitaxial growth of single-crystal SLG from multiple nuclei. (B,C) Scanning electron microscope images of aligned graphene islands and a continuous single-crystal graphene film grown on the home-made Cu(111) foils. The inset in (C) is a low-energy electron diffraction (LEED) pattern (beam size  $\approx 1$  mm) of an adlayer-free graphene film on a Cu(111) foil. (D–I) Several characterizations for the crystallinity of graphene films grown on home-made Cu(111) and Cu/Ni(111) foils, including (D) scanning tunneling microscopy (STM) image, (F) representative micro-LEED patterns (beam size of 23  $\mu$ m), (G) distribution of graphene lattice orientation angles determined from micro-LEED patterns at 2500 different positions, (H) representative selected area electron diffraction patterns, and (I) high-resolution transmission electron microscopy image. (E) The atomic structure of an adlayer-free single-crystal graphene film on a Cu(111) foil, showing a Moiré periodicity of  $\sim 6.4$  nm. The inset in (D) is the fast Fourier transform pattern of the STM image. (J) Schematic of the system for a reported continuous and ultrafast growth of meter-scale single-crystal graphene film and photograph of Cu(111) foils with graphene coverage of  $\sim 60\%$  (top),  $\sim 90\%$  (middle), and  $\sim 100\%$  (bottom). (K) Photographs of a pilot-scale atmospheric pressure chemical vapor deposition furnace for scalable growth of single-crystal graphene wafers on Cu<sub>90</sub>Ni<sub>10</sub>(111) films. Image reproduced, with permission, from [25,54,70–72].

of subsurface carbon in the Cu foils that produces additional nuclei directly correlates with the extent of adlayer growth and high-temperature annealing in a  $\text{H}_2/\text{Ar}$  atmosphere is an efficient way to remove these subsurface carbon contaminants [59]. The single crystallinity of this adlayer-free SLG film was verified by many instruments, including STM, polarized optical microscopy, low-energy electron diffraction (LEED), and micro-LEED, as shown in Figure 4C–G. Centimeter-long parallel **graphene folds** are present in the adlayer-free SLG films (Figure 4C) and have an average width of 80–100 nm and an average separation of 20–50  $\mu\text{m}$ . By patterning graphene field effect transistors with the device channel in the ‘clean’ regions between adjacent folds, high-performance devices with carrier mobilities of around  $1.0 \times 10^4 \text{ cm}^2 \text{ V}^{-1} \text{ s}^{-1}$  have been achieved without the disturbance of adlayers, GBs, and folds, which are all found to decrease the carrier mobilities. Using the camphor-assisted transfer method, the mechanical properties of a centimeter-scale single-crystal graphene film were measured, revealing a Young’s modulus of 728–908 GPa and an average fracture strength of 4.5 GPa [25]. Such a graphene film, without any GBs and adlayers, is essential for constructing ‘stacked graphene single crystals’ with controlled rotation angles and number of layers by a layer-by-layer assembly method, which we will discuss later.

Epitaxial growth of large single-crystal SLG films has been reported after 5 min of growth on centimeter-scale Cu/Ni(111) foils with Ni concentrations ranging from 1.3 at.% to 8.6 at.% [54]. High-resolution transmission electron microscopy (HRTEM), SAED patterns and  $\text{H}_2$  etching are used to investigate the crystallinity of the as-grown single-crystal SLG film (Figure 4H,I). This fast growth of single-crystal graphene due to the significantly lower energies of: (i) the barrier to methane dehydrogenation, and (ii) the formation of active carbon species on a Cu/Ni(111) surface, compared with a Cu(111) surface [54]. Xu and colleagues reported a single-crystal SLG film over  $5 \times 50 \text{ cm}$  achieved in 20 min by combining oxide-assisted CVD method and roll-to-roll technique (Figure 4J) [70]. A scalable growth of 25 pieces of 4-inch single-crystal graphene films on  $\text{Cu}_{90}\text{Ni}_{10}$ (111) films has been reported by a home-designed CVD system by Deng and colleagues (Figure 4K) [71].

Very recently, Wu and Li independently reported the preparation of large-area single-crystal high-index Cu surfaces [77,78]. Epitaxial growth of graphene has been reported on various indices, such as 112, 311, and 436 [77–79]. Density function theory calculations indicated that this is due to the single lowest energy state of graphene nucleation on high-index Cu surface [79]. These reported results of large-area single-crystal graphene films on copper-based substrates with a variety of surface orientations may open new opportunities. In addition, melted copper has been reported as the substrate for the growth of single-crystal SLG films. Fu and colleagues reported the seamless stitching of neighboring round graphene islands on liquid copper due to a self-rotation process on the smooth surface of liquid copper [80], while Yu and colleagues reported aligned hexagonal graphene islands grown in the temperature range 1083–1140°C, and theoretical calculations indicated that the aligned islands were driven by gas flow [81]. However, temperatures higher than the melting point of Cu, 1084.6°C, and tungsten foils, are needed to melt and support the copper.

Unlike the single-nucleus method, which often needs a very low flow rate of the carbon precursor to suppress density of the nucleation of graphene, the parametric window of growth of single-crystal graphene on single-crystal Cu(111) and Cu/Ni(111) substrates is reportedly much broader, resulting in both a faster growth rate and higher repeatability, which makes the multiple-nuclei method likely to be more promising for mass production. It should be noted that 1–2% misorientation of graphene islands is usually observed in as-grown single-crystal SLG films by this multiple-nuclei method, which may be due to impurities or artifacts on the substrate surface [68,70].

## Synthesis of Single-Crystal BLG

Although the growth of single-crystal SLG has been well studied, studies of the growth of BLG on Cu-based substrates, whether or not it is single crystal, are inadequate. The size of BLG grown on Cu substrates is limited by the surface-mediated growth mechanism [21]. That is, once the surface of the Cu substrate is fully covered by graphene, the decomposition of CH<sub>4</sub> on the metal surface typically stops, as well as the growth of both layers. Despite many strategies being reported to break the surface-mediated mechanism and increase the coverage of the second layer, including using a more active carbon precursor such as ethane or ethanol [82,83], using a dynamic **CVD protocol** [84], and providing additional catalyst [85], it is still challenging to produce continuous BLG films with 100% coverage. Similar to the single-crystal SLG growth methods, there are two reported strategies for the growth of large-area single-crystal BLG: (i) growth from one single nucleus, and (ii) epitaxial growth from multiple nuclei. Using layer-by-layer transfer, single-crystal SLG has been reportedly used to form BLG with a defined angle between the layers [86] (see Table 2).

### Single-Crystal BLG Grown from One Single Nucleus

It is more challenging to produce large-area single-crystal BLG than SLG from one single nucleus because one not only needs to control the nucleation density, as for SLG, but also find a way to

Table 2. Representative Studies on the Synthesis of Large-Area Single-Crystal Bi- and Multilayer Graphene

Strategy	Reported mechanism	Reported substrate	Reported size/coverage	Reported growth time	Reported stacking order	Year	Refs
Single nucleus	Surface diffusion	Poly-Cu	300 μm	24 h	AB-stacked	2013	[87]
		Poly-Cu enclosure	410 μm	3 h	AB-stacked	2013	[93]
		Poly-Cu	<100 μm	115 min	30°-twisted	2014	[95]
		Poly-Cu	540 μm	5–6 h	AB-stacked	2015	[88]
		Poly-Cu	10–20 μm	40 min	4°, 5°, 8°, 10.5°, 13°, 16°, 21°, 27°, 29°-twisted	2016	[99]
		Melted Cu	~100 μm	8 min	30°-twisted	2017	[96]
	Diffusion through the metal bulk	O-rich poly-Cu enclosure	550 μm	6 h	AB-stacked	2016	[29]
	Segregation from Cu/Ni alloy	Poly-Cu <sub>85</sub> Ni <sub>15</sub> foils	300 μm	10 min	AB-stacked	2016	[90]
Cu/Ni(111) foils with 23–28 at.% Ni		150–310 μm multilayer graphene islands with 3–8 layers	10 min	ABA... stacked	2020	[91]	
Multiple nuclei	Segregation from Cu/Ni alloy	Cu/Ni(111) foils with 16.6 at.% or 20.3 at.% Ni	1 × 2 cm <sup>2</sup> with more than 95% BLG or 60% TLG <sup>a</sup>	10 min	Almost 100% AB for BLG and almost 100% ABA for TLG	2020	[91]
		Cu/Ni(111) film with 23 at.% Ni	3 × 5 cm <sup>2</sup> with 99.4% BLG	10 h	99.4% AB	2020	[103]
	Sublimation of Si from Cu-Si alloy	Cu-Si film with 28.7 at.% Si	2 inch with 100% BLG, 100% TLG, or 100% tetralayer graphene	10 min	100% AB for BLG, 100% ABA for TLG, and 80% ABCA + 20ABAB for tetralayer graphene	2020	[104]
Layer-by-layer assembly	Stacking aligned hexagonal graphene islands and SLG films grown on Cu(111) films		2 cm	–	AB-stacked	2016	[114]
	Folding a single-crystal SLG grown on a Cu(111) foil		Millimeter scale	–	Arbitrary angle	2017	[115]

<sup>a</sup>Abbreviation: TLG, trilayer graphene.

continuously feed the carbon for the growth of the second layer. Methods used to decrease the nucleation density for SLG, such as using a high  $\text{H}_2/\text{CH}_4$  ratio (or low partial pressure of  $\text{CH}_4$ ) and introducing surface oxygen, are also reported to work well for BLG growth [29,87]. Three methods to break the limitation of a surface-mediated mechanism and feed carbon atoms to build the second layer are discussed later: (i) surface diffusion in the interface between the top layer (marked as the first layer) and the Cu substrate (Figure 5A) [87,88]; (ii) diffusion through the metal substrate from its back side (Figure 5F) [29,89]; and (iii) segregation/precipitation from Cu/Ni alloys [90]. The advantages and disadvantages of this single-nucleus strategy for single-crystal BLG growth are similar to those of SLG grown from a single nucleus, that is, it is not necessary to use a single-crystal substrate, but the growth rate is usually very low. And, if using single crystal Cu/Ni(111) alloy as the substrates, single crystal multilayer graphene islands with three to eight layers and sizes of more than 150  $\mu\text{m}$  have been reported [91].

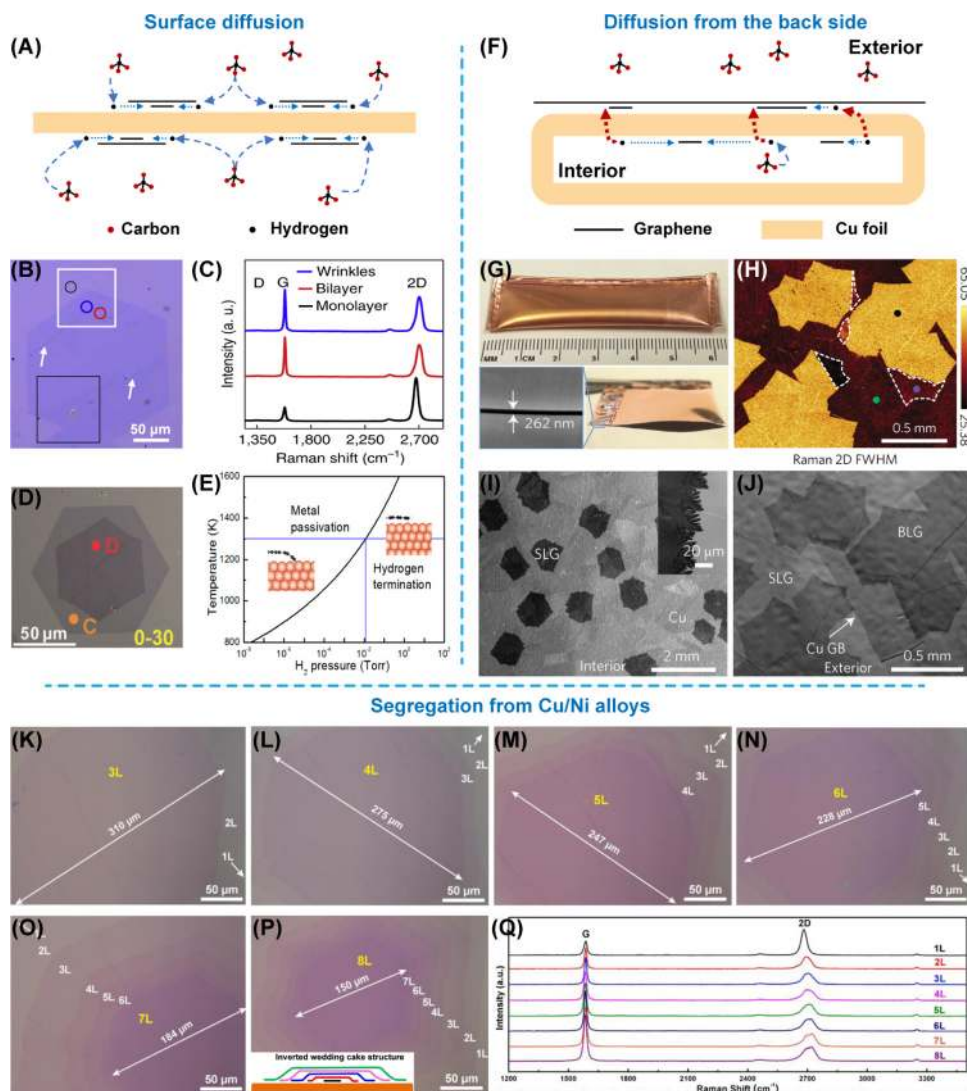
#### *Carbon Atoms Build the Second Layer by Surface Diffusion*

In 2013, Zhou and colleagues reported a 300- $\mu\text{m}$  AB-stacked single-crystal BLG island in 24 h on a polycrystalline Cu foil. They preoxidized the Cu foil to decrease the nucleation density and used a  $\text{H}_2/\text{CH}_4$  molar ratio of 4400 to suppress the growth of the first layer and offer more time to increase the size of the second layer before full coverage of the first SLG (Figure 5B,C) [87]. The role of hydrogen in the growth of BLG was investigated by theoretical simulation [92]. It was reported that the graphene edges detach from the metal surface and become terminated by H at a high partial pressure of hydrogen, which favors the diffusion of active carbon species into the space between the first layer and the metal substrate surface to form the second layer under the first (Figure 5E). Using a low  $\text{CH}_4$  partial pressure inside a Cu pocket, Li and colleagues reported a 410- $\mu\text{m}$  AB-stacked BLG island on the interior surface of the pocket [93]. They reported that the second layer grows simultaneously and under the first graphene layer. It was also reported that the growth of the second layer is nearly an order of magnitude slower than that of the first layer, because the active carbon species that are stated to contribute to the growth of the second layer have to diffuse across the edge of the first layer.

Besides the dominant stacking mode (AB-stacking), 30°-twisted BLG has been reported in certain studies of growth on Cu substrates [94]. Why 30°-twisted BLG is obtained is under discussion [95–98]. Yan and Deng reported that Cu steps may serve as the nucleation sites for the second layer [95,97]; they suggest that the zigzag and armchair edges of graphene can efficiently saturate the Cu step atoms on Cu(111), resulting in 0° and 30° orientations related to the Cu lattice. Quasicrystal 30°-twisted BLG islands with sizes of around 100  $\mu\text{m}$  have been reported on a polycrystalline copper foil (Figure 5D). Li and colleagues reported 30°-twisted BLG islands grown on melted Cu and proposed that the interaction between two graphene layers should be responsible for the preference of AB-stacked and 30°-twisted BLG [96]. BLG islands grown on Cu with twist angles such as 4°, 13°, and 21° have been reported [99]. Their sizes were in the order of tens of microns and they were a small fraction of the as-grown BLG, relative to the much higher preponderance of AB-stacked and 30°-twisted BLG. Obtaining reliable and reproducible growth of large-area twisted BLG with desired twist angle is an important and exciting challenge for the future.

#### *Carbon Atoms Diffuse through the Metal Substrate from Its Back Side*

Another way to feed carbon atoms is to create asymmetric growth environments on the two sides of the Cu substrate. For example, different methane concentrations on the two sides will result in different growth rates and graphene coverage. Hao and colleagues first reported a half-millimeter AB-stacked BLG island using a Cu pocket made from a polycrystalline oxygen-rich Cu foil (Figure 5G) [29]. It was reported that the exterior surface of the pocket was covered by a



Trends in Chemistry

Figure 5. Three Typical Strategies for Growing Single-Crystal Bilayer Graphene (BLG) Islands by the Single-Nucleus Method. (i) Feeding carbon atoms for the growth of the second layer by surface diffusion (A), (ii) diffusing the carbon atoms through the metal substrate from its back side (F), and (iii) segregating/precipitating carbon atoms from Cu/Ni alloys. (B) Optical image of the AB-stacked BLG island grown using a high  $H_2/CH_4$  ratio of 4400, which was then transferred to a 300-nm  $SiO_2/Si$  wafer. (C) Raman spectra taken from the spots marked with the corresponding colored circles in (B). (D) Optical image of twisted bilayer graphene islands grown on a polycrystalline Cu surface then transferred to a 300-nm  $SiO_2/Si$  wafer. (E) Diagram of graphene zigzag edge formation on the Cu(111) surface at different hydrogen pressures and growth temperatures. (G) Optical image of the Cu pocket. (I, J) Scanning electron microscope images of graphene islands grown on the interior (I) and exterior (J) surfaces of an oxygen-rich Cu pocket. (H) Raman map of the full width at half maximum (FWHM) of the 2D band for the area in (J). (K–P) Optical images of graphene islands with (K) three layers, (L) four layers, (M) five layers, (N) six layers, (O) seven layers, and (P) eight layers grown on Cu/Ni(111) foils with 23–28 at.% Ni then transferred to 300-nm  $SiO_2/Si$  wafers. The inset in (P) is a schematic of the ‘inverted wedding cake’ structure of multilayer graphene. (Q) Raman spectra of hexagonal multilayer graphene domains on 300-nm  $SiO_2/Si$  wafers. Images adapted, with permission, from [29,87,91,92,95]. Abbreviations: GB, grain boundary; SLG, single-layer graphene.

continuous graphene layer with large BLG islands (300–550  $\mu m$ ), while only isolated SLG islands were observed with a low density of  $\sim 0.5\text{ mm}^{-2}$  on the interior surface even after growth for 6 h, leaving more than 60% of the Cu surface exposed (Figure 5H–J). Using carbon isotope labeling,

the second layer of the BLG islands has been shown to be formed by carbon atoms diffusing through the foil from the interior surface, rather than by the precipitation/segregation of carbon from the metal bulk. The extremely low  $\text{CH}_4$  partial pressure inside the pocket is reportedly essential for decreasing the nucleation density of both the SLG islands on the interior surface and the second layer islands on the exterior surface. In this case, the authors proposed that oxygen on the interior surface not only passivates the graphene nucleation to achieve a low coverage of graphene on the interior surface but also promotes the decomposition of  $\text{CH}_4$  on the exposed Cu regions, resulting in a concentration gradient of active carbon species from the interior to the exterior surface, which drives the carbon diffusion through Cu bulk to the exterior surface for the growth of the second layer [100]. Unlike the surface-diffusion mechanism, the second layer is reported to nucleate later than the first layer [29,100].

It should be noted that the first continuous layer on the exterior surface is reportedly polycrystalline since it was grown from multiple nuclei on the polycrystalline Cu foil, so single-crystal AB-stacking will not be maintained when the single-crystal second layer grows across the GBs of the first layer. It was also reported that the second layer prefers to stack in the AB sequence with the layer under which it nucleated, so GBs form when two of these islands merge because they nucleated under islands with different orientations. Using a pocket made from a single-crystal Cu(111) foil might be helpful in producing a large-area single-crystal AB-stacked BLG film by the seamless stitching of second layer islands.

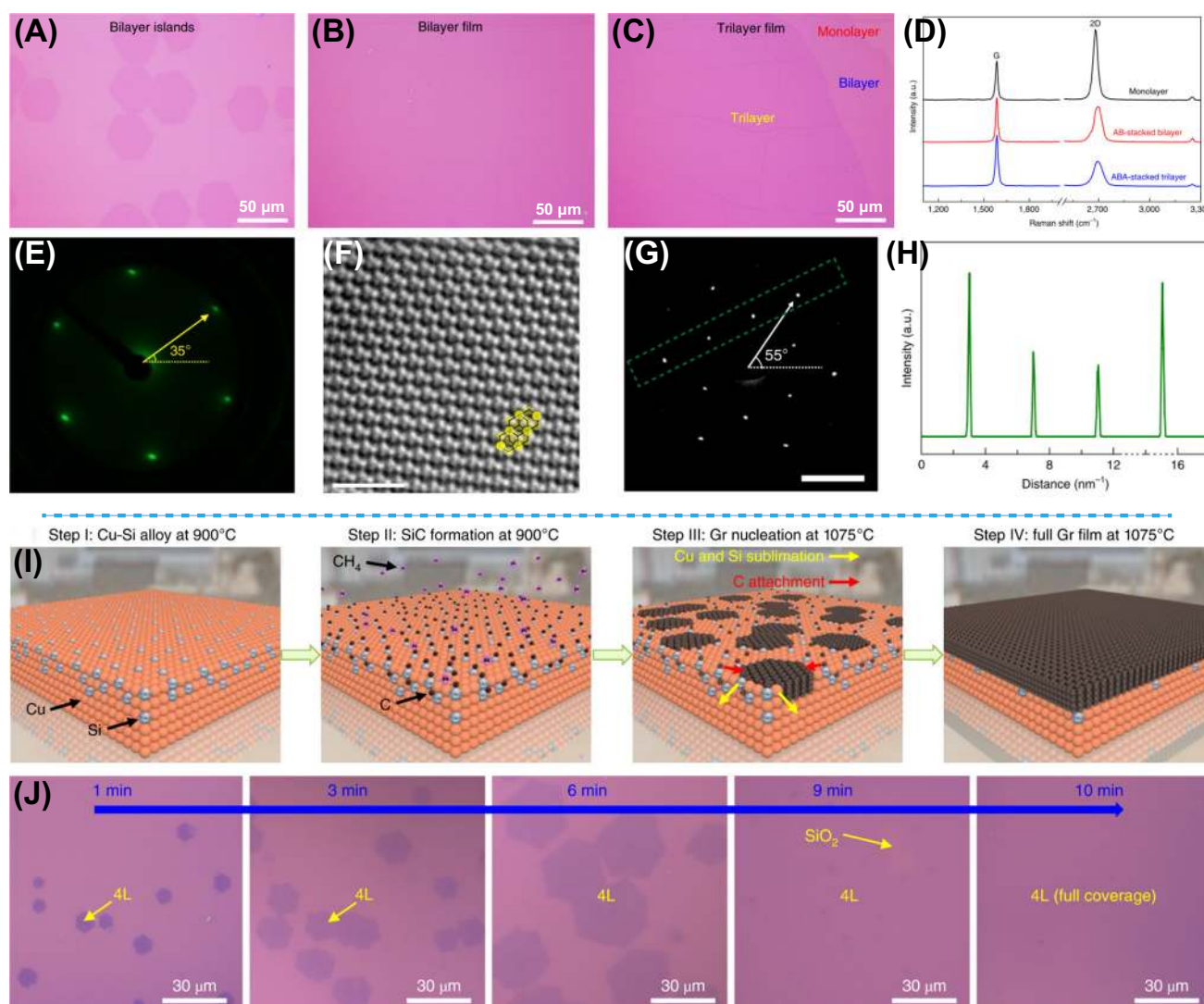
#### Carbon Atoms Segregate/Precipitate from the Cu/Ni Metal Bulk

As mentioned earlier, Cu/Ni foils or films show reported advantages by providing a low nucleation density and a fast growth rate. In addition, the carbon solubility in the Cu/Ni alloy is reported to be controllable by changing the concentration of Ni [101] and the dissolved C atoms can serve as the carbon source for the growth of the second layer. Yang and colleagues reported a 300- $\mu\text{m}$  single-crystal AB-stacked BLG island on a polycrystalline  $\text{Cu}_{85}\text{Ni}_{15}$  foil in a copper-vapor-assisted growth [90]. A copper foil was placed on the top of the Cu/Ni substrate with the stated goal of generating copper vapor at 1075°C, which reportedly inhibited catalysis of the Cu/Ni surface and reduced the growth rate of the first layer so as to provide more time for C atoms to diffuse into the Cu/Ni substrates. Recently, Huang and colleagues reported multi-layer hexagonal single-crystal graphene islands with three to eight layers and sizes of more than 150  $\mu\text{m}$  on Cu/Ni(111) foils with 23–28 at.% Ni, as shown in Figure 5K–P [91]. The reported Raman spectra indicated that these multilayers were stacked in ABA... modes (Figure 5Q). It was reported that these multilayer graphene regions were stacked in an ‘inverted wedding cake’ configuration (Figure 5P), confirmed by three independent methods (depth profiling of time-of-flight secondary ion mass spectrometry, environmental scanning electron microscopy with hydrogen etching, and cross-section transmission electron microscopy).

#### Single-Crystal BLG Grown from Multiple Nuclei

Similar to the growth of SLG, a single-crystal large-area BLG film can also be obtained by merging aligned BLG islands. To continuously supply carbon atoms for the growth of the second layer, Cu/Ni(111) substrates have been studied for the growth of single-crystal BLG films. Takesaki and colleagues reported the growth of a highly uniform graphene film with 93% BLG coverage on an epitaxial  $\text{Cu}_{77}\text{Ni}_{22}$  thin film, in which around 70–80% BLG was AB-stacked [102]. Recently, the same group reported an improvement of a 99.4% AB-stacked graphene film with similar BLG coverage by extending the growth time to 10 h at an elevated growth temperature (1085°C) and they proposed that the twisted second layer was transformed to AB-stacked by carbon dissolution-segregation processes [103]. Huang and colleagues reported that a centimeter-scale, almost 100% AB-stacked single-crystal graphene film, with 95% bilayer coverage, was produced on a

home-made Cu/Ni(111) alloy with 16.6 at.% Ni (Figure 6A,B), while the growth of an ABA-stacked (almost 100%) graphene film with 60% trilayer coverage was achieved on a Cu/Ni(111) alloy with 20.3 at.% Ni (Figure 6C,D) [91]. The results of isotope labeling indicated that the graphene grown on Cu/Ni(111) foils with 16.6 at.% Ni was predominantly driven by the segregation of carbon adatoms from the bulk. The single crystallinity of as-grown BLG film was verified by SAED, HRTEM, and LEED, as shown in Figure 6E–H. However, it is still very difficult to control the uniformity of the number of graphene layers over a large area because undesired multilayer patches usually appear due to the segregation growth mechanism.



Trends in Chemistry

**Figure 6. Strategies for the Production of Single-Crystal Bilayer Graphene (BLG) Films by the Multiple-Nuclei Method.** (A–C) Optical images of (A) aligned BLG islands, (B) a BLG film, and (C) a trilayer graphene film grown on Cu/Ni(111) foils then transferred to 300-nm SiO<sub>2</sub>/Si wafers. (D) Raman spectra of single-layer graphene, AB-stacked BLG, and ABA-stacked trilayer graphene. (E–H) Results of several characterizations for the crystallinity of BLG films grown on home-made Cu/Ni(111) foils, including (E) low-energy electron diffraction pattern, (F) high-resolution transmission electron microscopy image, (G) selected area electron diffraction (SAED) pattern, and (H) intensity profile of the diffraction spots along the green broken line in the representative SAED pattern shown in (G). (I) Growth steps of multilayer graphene on Cu-Si alloy. (J) Optical images showing the time evolution of tetralayer graphene grown on Cu-Si alloy films, then transferred to SiO<sub>2</sub>/Si wafers. Images adapted, with permission, from [91,104]. Abbreviations: Gr, graphene. 4L, tetralayer graphene.

Very recently, Nguyen and colleagues reported the layer-controlled growth of wafer-scale uniformly oriented graphene layers on Cu-Si alloy films, including AB-stacked bilayer, ABA-stacked trilayer, and ABCA-stacked tetralayer graphene films (Figure 6I,J) [104]. A wafer-scale ( $\sim 1.5 \times 3.5 \text{ cm}^2$ ) polycrystalline AB-stacked BLG film reportedly grown on a liquid  $\text{Pt}_3\text{Si}$ /solid Pt substrate was recently published [105]. These papers suggest that certain M-Si alloys could be a useful substrate for the growth of large-area multilayer graphene.

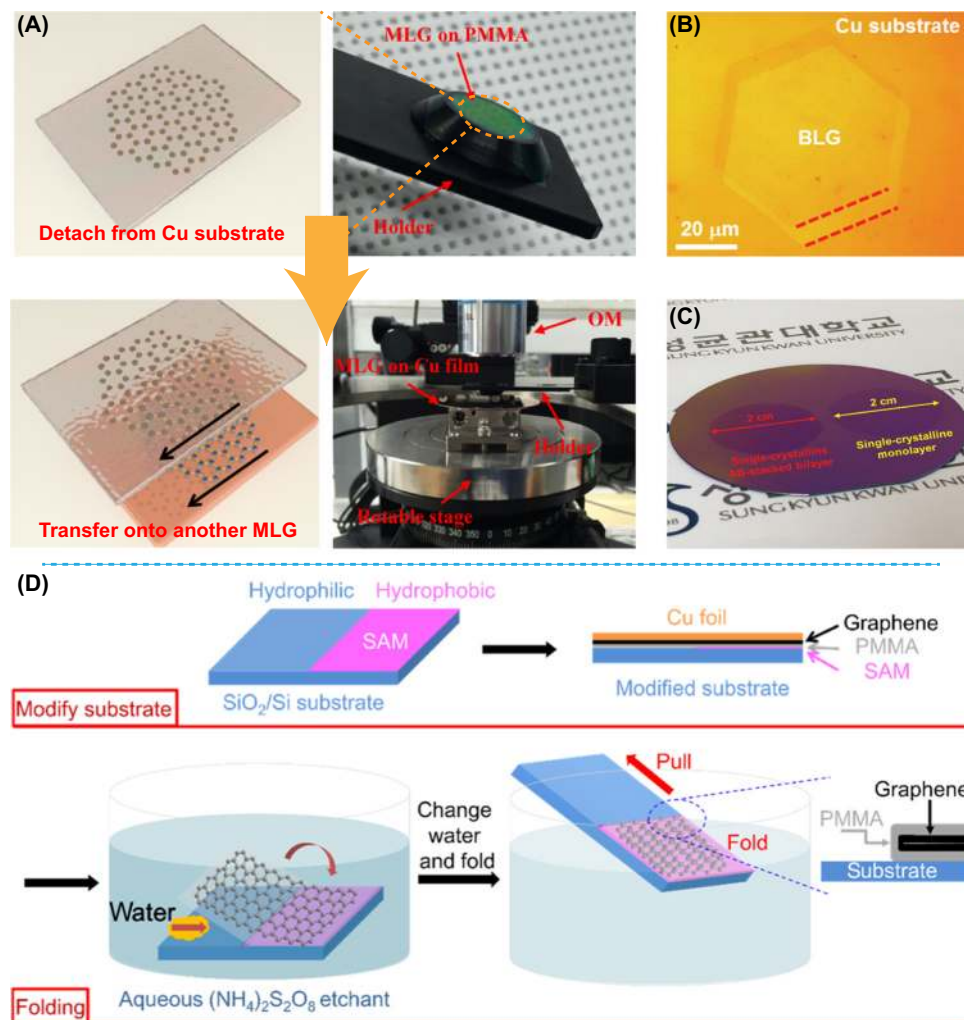
Even though the ‘inverted wedding cake’ configuration of bilayer/multilayer graphene grown on Cu and Cu/Ni substrates has been reported in the literature using many methods, this does not mean that it is impossible to grow the second layer on top of the first layer [29,72,91,93]. Extra Cu foils [106] or a partially exposed Cu surface [107] region upstream have been reported to be beneficial for the decomposition of  $\text{CH}_4$ , providing a continuous supply of carbon fragments to the downstream, resulting in an increased BLG coverage there. Since the Cu foils used in both reports are polycrystalline, the authors did not get single-crystal BLG. Stronger evidence (e.g., isotope labeling) is needed to confirm that the second layer grows on top of the first layer.

#### Layer-by-Layer Assembly of Single-Crystal SLG

Layer-by-layer assembly has been used to produce van der Waals heterostructures of 2D materials [108,109]. Unlike direct growth by the CVD method, contaminants may be introduced into the interface of two graphene layers during the transferring and stacking processes, which is reported to decouple the two graphene layers and decrease the carrier mobilities and thermal conductivity of the stacked BLG [110,111]. Viscoelastic stamps (including polydimethylsiloxane and epoxy) and h-BN have been reportedly used as the support materials for transferring and stacking exfoliated graphene sheets without any treatments by solvents or solutions [108,112]. Since the exfoliated graphene is usually in irregular shapes with an unknown crystallographic orientation, Kim and Chen divided one graphene sheet into two parts by tearing or laser cutting, then stacked these two parts with a defined rotation angle [112,113]. The BLG is a few micrometers in size. We might expect that ‘clean dry transfer’ will continue to advance and perhaps lead to assembly of significantly larger layers with clean interfaces. Since large-area single-crystal SLG films can now be readily obtained, their layer-by-layer assembly seems a promising way to produce single-crystal (or quasicrystal) bilayer or even multilayer graphene with controlled stacking angles. This layer-by-layer assembly requires: (i) that the single-crystal SLG should not contain any adlayers over a large area, (ii) rapid nondestructive identification of the lattice orientation of the single-crystal SLG, and (iii) a well-developed graphene transfer method that does not introduce any residue and contaminants to the interfaces between the graphene layers during the stacking.

Nguyen and colleagues reported a single-crystal AB-stacked BLG island by transferring a hexagonal single-crystal SLG island to the top of the other SLG island, resulting in a polymer-free interface between the two graphene layers, as shown in Figure 7A–C [114]. The orientation angle was reported to be precisely controlled by an optical microscope with assistance of a micromanipulator and a rotatable stage. The authors noted that a tiny misalignment ( $\sim 1^\circ$ ) can be removed by annealing the resulting BLG sample at  $350^\circ\text{C}$ , because thermal energy drives local lattice relaxation to form the BLG minimum energy state AB-stacking.

Ruoff and colleagues have reported a millimeter-scale BLG film with a defined twist angle between the layers that was obtained by folding a continuous single-crystal SLG film [115]. As shown in Figure 7D, after transferring the adlayer-free single-crystal SLG film onto a tailored substrate that had hydrophilic and hydrophobic regions patterned by a layer of self-assembled molecules, the graphene film in these two regions would ‘self-fold’ when the substrate was



Trends in Chemistry

Figure 7. Two Typical Strategies for the Production of Single-Crystal Bilayer Graphene (BLG) by Layer-by-Layer Assembly with Specific Rotation Angles. (A) Stacking hexagonal single-layer graphene (SLG) islands with assistance of an optical microscope (OM) with a rotatable stage and micromanipulator, and (D) directly folding a single-crystal monolayer graphene (MLG) film into a BLG film with the desired twist angle. (B) Optical image of AB-stacked BLG on a Cu substrate. (C) Photograph of the original single-crystal SLG and the synthesized single-crystal AB-stacked BLG with a diameter of 2 cm. Images adapted, with permission, from [114,115]. Abbreviations: PMMA, polymethyl methacrylate; SAM, self-assembled monolayer.

withdrawn from water, resulting in macroscopic folded graphene with good uniformity. The fold line can be adjusted by controlling the borders between the hydrophobic/hydrophilic regions and it was found that this correlated with the twist angle of the prepared BLG. By using a LEED pattern to identify the original lattice orientation of the SLG on the Cu(111) foil, or establishing the relation between the fold angle and the twist angle, a tBLG film with a defined stacking orientation (with a standard error of  $\sim 0.25^\circ$ ) was achieved.

Apart from this manual way of stacking graphene layers, a structural directing effect of a single-crystal SLG film on the carbonization and graphitization of polymer thin films has been reported recently by Ruoff and colleagues. By embedding a single-crystal SLG film in an SU-8

(an epoxy-based negative photoresist) film and subsequently heating it in an inert atmosphere, oriented graphene-like layers formed by graphitization of the polymer appeared in the SU-8 near the graphene at 1000°C, at which graphitization usually does not happen, whereas no graphitization occurred away from the single-crystal graphene. This observation strongly proves the catalytic influence of graphene on the carbonization and graphitization of polymers, indicating a potential method for the synthesis of single-crystal graphite [116].

## Concluding Remarks

Even given significant effort by a number of groups worldwide for the synthesis of single-crystal graphene, there remain imperfections in nearly all of the CVD-grown single-crystal graphene that has been reported (see Outstanding Questions). For example, wrinkles and folds are usually present in CVD-grown single-crystal graphene films but they are often mis-assigned or even ignored in the literature. Reliable methods for the complete elimination of wrinkles and/or folds are still under investigation. Imperfections such as pinholes, cracks, and impurities can be introduced during the graphene transfer process and reportedly degrade the performance of single-crystal graphene [117]. New graphene transfer methods are called for to maintain the physical integrity of the graphene over a large area and to avoid introducing impurities or residue on the surface(s) of graphene films. The direct growth of high-quality single-crystal graphene on, for example, dielectric substrates used in electronic devices, is thus of interest. These are important and interesting challenges, also for achieving certain applications of single-crystal graphene.

The precise control of the number of layers of single-crystal graphene on copper over a large area for 2-, 3-, and  $n$ -layer ( $n = 4\text{--}10$ ) has not been achieved. New strategies are needed to grow a second layer on top of adlayer-free SLG, but with new precursors that favor growth of the second layer without forming a third layer in some regions and without etching the first layer.

The layer-by-layer assembly of adlayer-free single-crystal graphene films could be a viable method for producing large area multilayer graphene films with a specific number of layers and defined stacking angles. We call this material an ‘artificial graphene single crystal’ because it cannot be made by any direct growth method. This aspect is highly exciting, but at present pure speculation. As we mentioned earlier, a nondestructive and clean transfer method is in high demand.

## Acknowledgments

We acknowledge the support from the Institute for Basic Science (IBS-R019-D1).

## References

- Balandin, A.A. *et al.* (2008) Superior thermal conductivity of single-layer graphene. *Nano Lett.* 8, 902–907
- Lee, C. *et al.* (2008) Measurement of the elastic properties and intrinsic strength of monolayer graphene. *Science* 321, 385
- Novoselov, K.S. *et al.* (2004) Electric field effect in atomically thin carbon films. *Science* 306, 666
- Novoselov, K.S. *et al.* (2005) Two-dimensional atomic crystals. *Proc. Natl. Acad. Sci. U. S. A.* 102, 10451–10453
- Bolotin, K.I. *et al.* (2008) Ultrahigh electron mobility in suspended graphene. *Solid State Commun.* 146, 351–355
- Fang, W. *et al.* (2015) A review of large-area bilayer graphene synthesis by chemical vapor deposition. *Nanoscale* 7, 20335–20351
- Park, C. *et al.* (2015) Electronic properties of bilayer graphene strongly coupled to interlayer stacking and an external electric field. *Phys. Rev. Lett.* 115, 015502
- Kim, K. *et al.* (2017) Tunable moiré bands and strong correlations in small-twist-angle bilayer graphene. *Proc. Natl. Acad. Sci. U. S. A.* 114, 3364–3369
- Zhang, Y. *et al.* (2009) Direct observation of a widely tunable bandgap in bilayer graphene. *Nature* 459, 820–823
- Cao, Y. *et al.* (2018) Correlated insulator behaviour at half-filling in magic-angle graphene superlattices. *Nature* 556, 80–84
- Cao, Y. *et al.* (2018) Unconventional superconductivity in magic-angle graphene superlattices. *Nature* 556, 43–50
- Bakharev, P.V. *et al.* (2020) Chemically induced transformation of chemical vapour deposition grown bilayer graphene into fluorinated single-layer diamond. *Nat. Nanotechnol.* 15, 59–66
- Koren, E. *et al.* (2016) Coherent commensurate electronic states at the interface between misoriented graphene layers. *Nat. Nanotechnol.* 11, 752–757
- Li, G. *et al.* (2010) Observation of Van Hove singularities in twisted graphene layers. *Nat. Phys.* 6, 109–113
- Nimbalkar, A. and Kim, H. (2020) Opportunities and challenges in twisted bilayer graphene: a review. *Nano-Micro Lett.* 12, 126
- Ding, Y. *et al.* (2016) Stacking-mode-induced reactivity enhancement for twisted bilayer graphene. *Chem. Mater.* 28, 1034–1039

## Outstanding Questions

Can ‘perfect’ very large-area single-crystal, single-layer, graphene films be achieved (be grown)?

Can ‘perfect’ large-area single-crystal AB-stacked bilayer graphene films be directly grown, truly ‘free’ of any regions that are not BLG?

Can ‘perfect’ large-area single-crystal AB-stacked  $n$ -layer graphene films be directly grown, truly ‘free’ of any regions that are not the specific value of  $n$  that is desired? That is: 100% trilayer, or 100% 4-layer, and so on.

Moderately large (sub-mm) single-crystal AB-stacked BLG has been achieved in which the ‘adlayer’ is between a continuous surface layer and the substrate. Can reliable growth of bilayer graphene but also  $n$ -layer as mentioned earlier, be achieved through growth ‘on top’ (atop) of a perfect single-crystal, SLG film?

Are there ‘completely new’ methods of synthesizing large-area and single-crystal graphene compared with existing methods? Some other chemical process?

How can large-area graphene be transferred by a process that always yields particularly clean graphene and does not introduce any tears or cracks in the transferred film.

Can (extremely rapid) ‘cut, pick, and place’ methods be employed, using, for example, large-area ‘perfect’ single-crystal SLG to generate any  $n$ -layer stacking, with desired interlayer twist angle between all adjacent layers, and for final products of the desired  $n$ -layer stack that are centimeter or larger in lateral dimensions? (The reader may please note that there are many questions ‘embedded’ in this question. How can the crystallographic orientation of the large-area single crystal be rapidly identified, how can the process be accelerated from perhaps a manual approach to one that is done entirely with robotics, and so on.)

17. Li, X. *et al.* (2016) Synthesis of graphene films on copper foils by chemical vapor deposition. *Adv. Mater.* 28, 6247–6252
18. Li, X. *et al.* (2009) Large-area synthesis of high-quality and uniform graphene films on copper foils. *Science* 324, 1312
19. Lander, J.J. *et al.* (1952) Solubility and diffusion coefficient of carbon in nickel: reaction rates of nickel-carbon alloys with barium oxide. *J. Appl. Phys.* 23, 1305–1309
20. López, G.A. and Mittemeijer, E.J. (2004) The solubility of C in solid Cu. *Scr. Mater.* 51, 1–5
21. Li, X. *et al.* (2009) Evolution of graphene growth on Ni and Cu by carbon isotope labeling. *Nano Lett.* 9, 4268–4272
22. Huang, P.Y. *et al.* (2011) Grains and grain boundaries in single-layer graphene atomic patchwork quilts. *Nature* 469, 389–392
23. Wu, Y. *et al.* (2013) Crystal structure evolution of individual graphene islands during CVD growth on copper foil. *Adv. Mater.* 25, 6744–6751
24. Yu, Q. *et al.* (2011) Control and characterization of individual grains and grain boundaries in graphene grown by chemical vapour deposition. *Nat. Mater.* 10, 443–449
25. Wang, B. *et al.* (2018) Camphor-enabled transfer and mechanical testing of centimeter-scale ultrathin films. *Adv. Mater.* 30, 1800888
26. Ma, T. *et al.* (2017) Tailoring the thermal and electrical transport properties of graphene films by grain size engineering. *Nat. Commun.* 8, 14486
27. Grantab, R. *et al.* (2010) Anomalous strength characteristics of tilt grain boundaries in graphene. *Science* 330, 946–948
28. Suk, J.W. *et al.* (2020) Impact of grain boundaries on the elastic behavior of transferred polycrystalline graphene. *Chem. Mater.* 32, 6078–6084
29. Hao, Y. *et al.* (2016) Oxygen-activated growth and bandgap tunability of large single-crystal bilayer graphene. *Nat. Nanotechnol.* 11, 426–431
30. Wang, H. *et al.* (2014) Lateral homoepitaxial growth of graphene. *CrystEngComm* 16, 2593–2597
31. Dong, J. *et al.* (2018) How graphene crosses a grain boundary on the catalyst surface during chemical vapour deposition growth. *Nanoscale* 10, 6878–6883
32. Zhang, X. *et al.* (2012) How the orientation of graphene is determined during chemical vapor deposition growth. *J. Phys. Chem. Lett.* 3, 2822–2827
33. Kim, H. *et al.* (2012) Activation energy paths for graphene nucleation and growth on Cu. *ACS Nano* 6, 3614–3623
34. Braeuninger-Weimer, P. *et al.* (2016) Understanding and controlling Cu-catalyzed graphene nucleation: the role of impurities, roughness, and oxygen scavenging. *Chem. Mater.* 28, 8905–8915
35. Han, G.H. *et al.* (2011) Influence of copper morphology in forming nucleation seeds for graphene growth. *Nano Lett.* 11, 4144–4148
36. Yan, Z. *et al.* (2012) Toward the synthesis of wafer-scale single-crystal graphene on copper foils. *ACS Nano* 6, 9110–9117
37. Chen, S. *et al.* (2013) Millimeter-size single-crystal graphene by suppressing evaporative loss of Cu during low pressure chemical vapor deposition. *Adv. Mater.* 25, 2062–2065
38. Mohsin, A. *et al.* (2013) Synthesis of millimeter-size hexagon-shaped graphene single crystals on resolidified copper. *ACS Nano* 7, 8924–8931
39. Li, X. *et al.* (2010) Graphene films with large domain size by a two-step chemical vapor deposition process. *Nano Lett.* 10, 4328–4334
40. Li, X. *et al.* (2011) Large-area graphene single crystals grown by low-pressure chemical vapor deposition of methane on copper. *J. Am. Chem. Soc.* 133, 2816–2819
41. Chen, X. *et al.* (2015) Chemical vapor deposition growth of 5 mm hexagonal single-crystal graphene from ethanol. *Carbon* 94, 810–815
42. Wang, H. *et al.* (2012) Controllable synthesis of submillimeter single-crystal monolayer graphene domains on copper foils by suppressing nucleation. *J. Am. Chem. Soc.* 134, 3627–3630
43. Hao, Y. *et al.* (2013) The role of surface oxygen in the growth of large single-crystal graphene on copper. *Science* 342, 720–723
44. Ding, D. *et al.* (2017) Behavior and role of superficial oxygen in Cu for the growth of large single-crystalline graphene. *Appl. Surf. Sci.* 408, 142–149
45. Gan, L. and Luo, Z. (2013) Turning off hydrogen to realize seeded growth of subcentimeter single-crystal graphene grains on copper. *ACS Nano* 7, 9480–9488
46. Guo, W. *et al.* (2016) Oxidative-etching-assisted synthesis of centimeter-sized single-crystalline graphene. *Adv. Mater.* 28, 3152–3158
47. Li, Q. *et al.* (2014) Controllable seeding of single crystal graphene islands from graphene oxide flakes. *Carbon* 79, 406–412
48. Wu, W. *et al.* (2011) Growth of single crystal graphene arrays by locally controlling nucleation on polycrystalline Cu using chemical vapor deposition. *Adv. Mater.* 23, 4898–4903
49. Jang, H.-S. *et al.* (2020) Toward scalable growth for single-crystal graphene on polycrystalline metal foil. *ACS Nano* 14, 3141–3149
50. Ding, D. *et al.* (2016) Spatially controlled nucleation of single-crystal graphene on Cu assisted by stacked Ni. *ACS Nano* 10, 11196–11204
51. Wu, T. *et al.* (2016) Fast growth of inch-sized single-crystalline graphene from a controlled single nucleus on Cu–Ni alloys. *Nat. Mater.* 15, 43–48
52. Vlassioudis, I.V. *et al.* (2018) Evolutionary selection growth of two-dimensional materials on polycrystalline substrates. *Nat. Mater.* 17, 318–322
53. Liu, Y. *et al.* (2018) How low nucleation density of graphene on Cu/Ni alloy is achieved. *Adv. Sci.* 5, 1700961
54. Huang, M. *et al.* (2018) Highly oriented monolayer graphene grown on a Cu/Ni(111) alloy foil. *ACS Nano* 12, 6117–6127
55. Wang, H. *et al.* (2016) Surface monocrystallization of copper foil for fast growth of large single-crystal graphene under free molecular flow. *Adv. Mater.* 28, 8968–8974
56. Lin, L. *et al.* (2016) Rapid growth of large single-crystalline graphene via second passivation and multistage carbon supply. *Adv. Mater.* 28, 4671–4677
57. Sun, X. *et al.* (2018) Graphene: low-temperature and rapid growth of large single-crystalline graphene with ethane (Small 3/2018). *Small* 14, 1870011
58. Xu, X. *et al.* (2016) Ultrafast growth of single-crystal graphene assisted by a continuous oxygen supply. *Nat. Nanotechnol.* 11, 930–935
59. Liu, C. *et al.* (2019) Kinetic modulation of graphene growth by fluorine through spatially confined decomposition of metal fluorides. *Nat. Chem.* 11, 730–736
60. Ago, H. *et al.* (2012) Catalytic growth of graphene: toward large-area single-crystalline graphene. *J. Phys. Chem. Lett.* 3, 2228–2236
61. Fogarassy, Z. *et al.* (2014) Dominantly epitaxial growth of graphene on Ni(111) substrate. *Appl. Surf. Sci.* 314, 490–499
62. Ogawa, Y. *et al.* (2012) Domain structure and boundary in single-layer graphene grown on Cu(111) and Cu(100) films. *J. Phys. Chem. Lett.* 3, 219–226
63. Murdock, A.T. *et al.* (2013) Controlling the orientation, edge geometry, and thickness of chemical vapor deposition graphene. *ACS Nano* 7, 1351–1359
64. Brown, L. *et al.* (2014) Polycrystalline graphene with single crystalline electronic structure. *Nano Lett.* 14, 5706–5711
65. Wu, R. *et al.* (2019) Edge-epitaxial growth of graphene on Cu with a hydrogen-free approach. *Chem. Mater.* 31, 2555–2562
66. Yuan, Q. *et al.* (2014) Edge-catalyst wetting and orientation control of graphene growth by chemical vapor deposition growth. *J. Phys. Chem. Lett.* 5, 3093–3099
67. Xu, Z. *et al.* (2020) Molecular dynamics simulation of graphene sinking during chemical vapor deposition growth on semi-molten Cu substrate. *NPJ Comput. Mater.* 6, 14
68. Nguyen, V.L. *et al.* (2015) Seamless stitching of graphene domains on polished copper (111) foil. *Adv. Mater.* 27, 1376–1382
69. Deng, B. *et al.* (2017) Wrinkle-free single-crystal graphene wafer grown on strain-engineered substrates. *ACS Nano* 11, 12337–12345
70. Xu, X. *et al.* (2017) Ultrafast epitaxial growth of metre-sized single-crystal graphene on industrial Cu foil. *Sci. Bull.* 62, 1074–1080

71. Deng, B. *et al.* (2019) Scalable and ultrafast epitaxial growth of single-crystal graphene wafers for electrically tunable liquid-crystal microlens arrays. *Sci. Bull.* 64, 659–668
72. Luo, D. *et al.* (2019) Adlayer-free large-area single crystal graphene grown on a Cu(111) foil. *Adv. Mater.* 31, 1903615
73. Jin, S. *et al.* (2018) Colossal grain growth yields single-crystal metal foils by contact-free annealing. *Science* 362, 1021
74. Zhang, X. *et al.* (2019) Epitaxial growth of 6 in. single-crystalline graphene on a Cu/Ni (111) film at 750 °C via chemical vapor deposition. *Small* 15, 1805395
75. Burton, O.J. *et al.* (2020) Integrated wafer scale growth of single crystal metal films and high quality graphene. *ACS Nano* 14, 13593–13601
76. Hu, B. *et al.* (2012) Epitaxial growth of large-area single-layer graphene over Cu(111)/sapphire by atmospheric pressure CVD. *Carbon* 50, 57–65
77. Li, Y. *et al.* (2020) Large single-crystal Cu foils with high-index facets by strain-engineered anomalous grain growth. *Adv. Mater.* 32, 2002034
78. Wu, M. *et al.* (2020) Seeded growth of large single-crystal copper foils with high-index facets. *Nature* 581, 406–410
79. Hou, Y. *et al.* (2020) Surface crystallographic structure insensitive growth of oriented graphene domains on Cu substrates. *Mater. Today* 36, 10–17
80. Zeng, M. *et al.* (2016) Isotropic growth of graphene toward smoothing stitching. *ACS Nano* 10, 7189–7196
81. Xue, X. *et al.* (2019) Gas-flow-driven aligned growth of graphene on liquid copper. *Chem. Mater.* 31, 1231–1236
82. Wassei, J.K. *et al.* (2012) Chemical vapor deposition of graphene on copper from methane, ethane and propane: evidence for bilayer selectivity. *Small* 8, 1415–1422
83. Zhao, P. *et al.* (2014) Equilibrium chemical vapor deposition growth of Bernal-stacked bilayer graphene. *ACS Nano* 8, 11631–11638
84. Luo, B. *et al.* (2016) Chemical vapor deposition of bilayer graphene with layer-resolved growth through dynamic pressure control. *J. Mater. Chem. C* 4, 7464–7471
85. Yang, Q. *et al.* (2017) Regulating surficial catalysis mechanism of copper metal by manipulating reactive intermediate for growth of homogenous Bernal-stacked bilayer graphene. *Adv. Mater. Interfaces* 4, 1700415
86. Robinson, J.T. *et al.* (2013) Electronic hybridization of large-area stacked graphene films. *ACS Nano* 7, 637–644
87. Zhou, H. *et al.* (2013) Chemical vapour deposition growth of large single crystals of monolayer and bilayer graphene. *Nat. Commun.* 4, 2096
88. Gan, L. *et al.* (2015) Grain size control in the fabrication of large single-crystal bilayer graphene structures. *Nanoscale* 7, 2391–2399
89. Fang, W. *et al.* (2014) Asymmetric growth of bilayer graphene on copper enclosures using low-pressure chemical vapor deposition. *ACS Nano* 8, 6491–6499
90. Yang, C. *et al.* (2016) Copper-vapor-assisted rapid synthesis of large AB-stacked bilayer graphene domains on Cu-Ni alloy. *Small* 12, 2009–2013
91. Huang, M. *et al.* (2020) Large-area single-crystal AB-bilayer and ABA-trilayer graphene grown on a Cu/Ni(111) foil. *Nat. Nanotechnol.* 15, 289–295
92. Zhang, X. *et al.* (2014) Role of hydrogen in graphene chemical vapor deposition growth on a copper surface. *J. Am. Chem. Soc.* 136, 3040–3047
93. Li, Q. *et al.* (2013) Growth of adlayer graphene on Cu studied by carbon isotope labeling. *Nano Lett.* 13, 486–490
94. Mogera, U. and Kulkarni, G.U. (2020) A new twist in graphene research: twisted graphene. *Carbon* 156, 470–487
95. Yan, Z. *et al.* (2014) Large hexagonal bi- and trilayer graphene single crystals with varied interlayer rotations. *Angew. Chem. Int. Ed.* 53, 1565–1569
96. Li, Y. *et al.* (2017) Tailoring graphene layer-to-layer growth. *Nanotechnology* 28, 265101
97. Deng, B. *et al.* (2020) Interlayer decoupling in 30° twisted bilayer graphene quasicrystal. *ACS Nano* 14, 1656–1664
98. Pezzini, S. *et al.* (2020) 30°-Twisted bilayer graphene quasicrystals from chemical vapor deposition. *Nano Lett.* 20, 3313–3319
99. Yin, J. *et al.* (2016) Selectively enhanced photocurrent generation in twisted bilayer graphene with van Hove singularity. *Nat. Commun.* 7, 10699
100. Zhao, Z. *et al.* (2015) Study on the diffusion mechanism of graphene grown on copper pockets. *Small* 11, 1418–1422
101. Chen, S. *et al.* (2011) Synthesis and characterization of large-area graphene and graphite films on commercial Cu-Ni alloy foils. *Nano Lett.* 11, 3519–3525
102. Takesaki, Y. *et al.* (2016) Highly uniform bilayer graphene on epitaxial Cu-Ni(111) alloy. *Chem. Mater.* 28, 4583–4592
103. Solís-Fernández, P. *et al.* (2020) Isothermal growth and stacking evolution in highly uniform Bernal-stacked bilayer graphene. *ACS Nano* 14, 6834–6844
104. Nguyen, V.L. *et al.* (2020) Layer-controlled single-crystalline graphene film with stacking order via Cu-Si alloy formation. *Nat. Nanotechnol.* 15, 1–7
105. Ma, W. *et al.* (2019) Interlayer epitaxy of wafer-scale high-quality uniform AB-stacked bilayer graphene films on liquid Pt3Si/solid Pt. *Nat. Commun.* 10, 2809
106. Yan, K. *et al.* (2011) Formation of bilayer Bernal graphene: layer-by-layer epitaxy via chemical vapor deposition. *Nano Lett.* 11, 1106–1110
107. Liu, L. *et al.* (2012) High-yield chemical vapor deposition growth of high-quality large-area AB-stacked bilayer graphene. *ACS Nano* 6, 8241–8249
108. Wang, L. *et al.* (2013) One-dimensional electrical contact to a two-dimensional material. *Science* 342, 614–617
109. Novoselov, K.S. *et al.* (2016) 2D materials and van der Waals heterostructures. *Science* 353, aac9439
110. Purdie, D.G. *et al.* (2018) Cleaning interfaces in layered materials heterostructures. *Nat. Commun.* 9, 5387
111. Hu, Z. *et al.* (2020) Stacking of exfoliated two-dimensional materials: a review. *Chin. J. Chem.* 38, 981–995
112. Kim, K. *et al.* (2016) van der Waals heterostructures with high accuracy rotational alignment. *Nano Lett.* 16, 1989–1995
113. Chen, X.-D. *et al.* (2016) High-precision twist-controlled bilayer and trilayer graphene. *Adv. Mater.* 28, 2563–2570
114. Nguyen, V.L. *et al.* (2016) Wafer-scale single-crystalline AB-stacked bilayer graphene. *Adv. Mater.* 28, 8177–8183
115. Wang, B. *et al.* (2017) Controlled folding of single crystal graphene. *Nano Lett.* 17, 1467–1473
116. Cunnning, B.V. *et al.* (2019) Structure-directing effect of single crystal graphene film on polymer carbonization and graphitization. *Mater. Horiz.* 6, 796–801
117. Liu, L. *et al.* (2015) Defects in graphene: generation, healing, and their effects on the properties of graphene: a review. *J. Mater. Sci. Technol.* 31, 599–606